11th International Conference on High-Energy Accelerators

Geneva, Switzerland, July 7–11, 1980

organized by the
European Organization for Nuclear Research (CERN), Geneva

sponsored by the
International Union of Pure and Applied Physics (IUPAP)

Proceedings edited by
W. S. Newman, CERN, Geneva

1980

Birkhäuser Verlag
Basel · Boston · Stuttgart

STATUS REPORT ON THE COLLIDING BEAM FACILITY VEPP-4

The VEPP-4 Group
Institute of Nuclear Physics, Novosibirsk, USSR.

ABSTRACT

The start-up of VEPP-4 is the main subject of the present report. Experiments were carried out at the energy of ψ and ψ' mesons. The maximum luminosity was 3×10^{28} cm^{-2} s^{-1} at an energy of 1.85 GeV. The resonance depolarization of a polarized beam allowed an absolute energy calibration to be made with an accuracy better than 1×10^{-4}. This made it possible to improve, by more than an order of magnitude, the accuracy of measuring the masses of ψ and ψ' mesons. The experiments in the region of the Y-meson family and with the use of the MD-1 detector have been scheduled to start this year. It should be added that the transverse magnetic field of this detector provides good possibilities for studying two-photon processes.

1. VEPP-4 INJECTION SCHEME[1)]

The 2 × 7 GeV colliding electron-positron storage ring VEPP-4 (Fig. 1) was built on the basis of the VEPP-3 device. In the modified scheme, VEPP-3 operates as a booster ring with a subsequent acceleration of the stored electron or positron beams. Injection in VEPP-3 is made from the synchrotron B-4 at an energy of 350 MeV with a repetition rate of 1 Hz. The electrons and positrons are injected into the synchrotron at an energy of 7 MeV. Positrons are produced by electron conversion with an energy of 45 MeV, the electrons being accelerated by a high-current linear accelerator. The specific feature of the accelerator is the Gyrokon-type high-frequency source (f = 430 MHz, P = 60 MW, Δt = 11 ms)[2)].

At the present time, such a cascade scheme for positron production provides an accumulation rate of about 0.1 mA/min in VEPP-4. The main way of increasing the accumulation rate

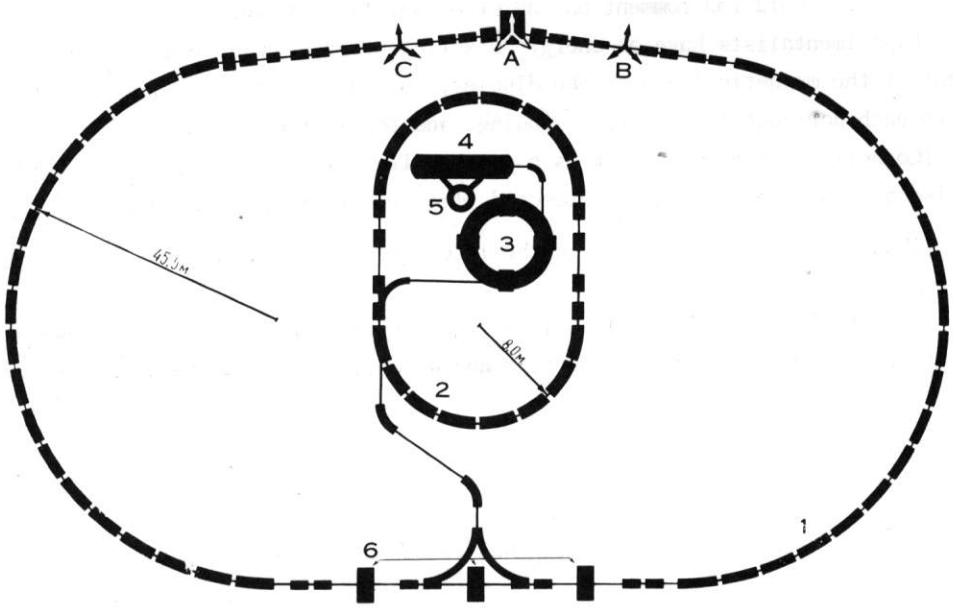

Fig. 1 A schematic view of VEPP-4. 1 - ring of VEPP-4; 2 - VEPP-3; 3 - synchrotron B-4; 4 - linear accelerator; 5 - pulsed Gyrokon; 6 - cavities.

is to decrease losses at all stages of accumulation and injection of the beams. Its realization enables the rate of positron accumulation to be increased up to 0.5 mA/min. The rate of electron accumulation is 1 mA/min.

For the accumulation of electrons and positrons in the ring of VEPP-4, in order to increase the acceptance, the injection system with a preliminary excitation of the stored beam is used, as has been done in the storage ring VEPP-2M [3]. All elements of the electron-optical channels (bending magnets, lenses, correction magnets) have a pulsed supply from unified generators. All systems of the injector and storage ring VEPP-4 are controlled by four computers ODRA-1325 on-line[4].

2. THE STORAGE RING VEPP-4

The storage ring VEPP-4 is composed of two semicircles with an average radius of 45 m and two straight sections between them. In one of the straight sections, 40 m long, there are the septum magnets, inflectors, and cavities; in the other, 55 m long, three interaction points with small β-functions are arranged. The magnetic detector with transverse magnetic field MD-1 [5], being a part of the storage ring magnetic structure, is installed at the central interaction point (A). The magnetic field of the detector and two additional magnets placed nearby enable an analysis to be made of the reaction products that escape at zero angle. At present, the detector MD-1 is undergoing adjustment (Fig. 2) and, instead of it, simple magnets are installed. The detector "OLYA"[6] is installed in one of two other symmetrically placed interaction points (B,C) with β_z = 15 cm. In the following we describe the first experiments carried out with this detector.

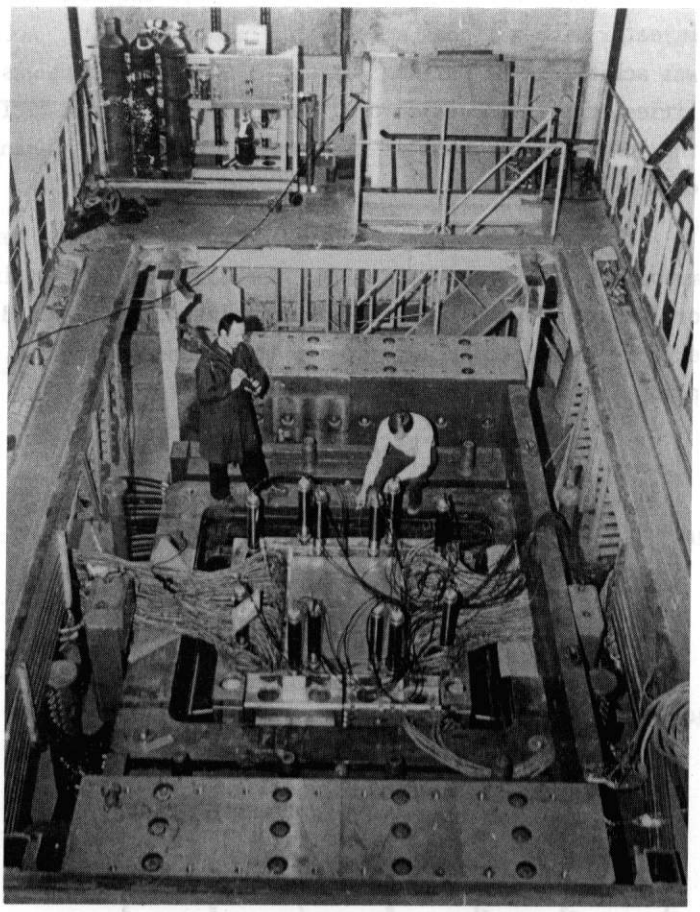

Fig. 2 The detector MD-1. The upper part of the magnetic circuit has been removed.

Regarding the systems for electrostatic separation of orbits, in the injection section the electron and positron orbits are always separated, and in the experimental section, separation is provided during the accumulation and acceleration periods.

The operating frequencies are the following: ν_z, ν_x = 9.1-9.3; the control is performed by means of the windings in the half-rings. Individual supply of the straight-section lenses allows the structure of the straight sections to be readjusted. There are also the sextupole lenses for chromaticity correction, and the skew quadrupoles for correction of the coupling resonances and the vertical η-function. There are 52 pick-up stations. The orbit is corrected to an accuracy of 1-2 mm. There are a large number of programs for operation with the magnetic system. The beam sizes are measured by means of synchrotron radiation.

Losses due to synchrotron radiation at an energy of 7 GeV are about 6 MeV. Because of the delay in starting the Gyrokon[7], which will provide this energy, the RF supply will be temporarily provided by tube generators. This enables one to start the experiments at E = = 5.5 GeV this year. At present, the maximum energy of about 3 GeV is provided by a single cavity.

The ring is pumped with magnetic charge/discharge pumps located inside and outside the vacuum chamber. The lifetime at a low current is over 10 hours; at a current of 10 mA it falls to 0.5 hours because of the internal scattering effect and outgassing due to synchrotron radiation.

3. LUMINOSITY

At the end of 1979 we came to perform two-beam experiments at VEPP-4 after the above injector with a linear accelerator had been built. Accumulation at an efficiency of 50-80% was achieved, the maximum current in a single bunch was 5 mA. To suppress transverse instabilities, the introduction of a small positive chromaticity turned out to be sufficient, while the longitudinal instabilities were suppressed by tuning the frequency of the highest harmonics of the cavity.

The two-beam regime was studied in considerable detail at the energies of ψ and ψ' mesons (E = 1.55 and 1.84 GeV). Operation was accomplished at one interaction point; the orbits at the opposite interaction point were separated. Note that this separation must be exactly localized because even a small non-compensated separation at the main interaction point leads to an increase in beam sizes (Fig. 3).

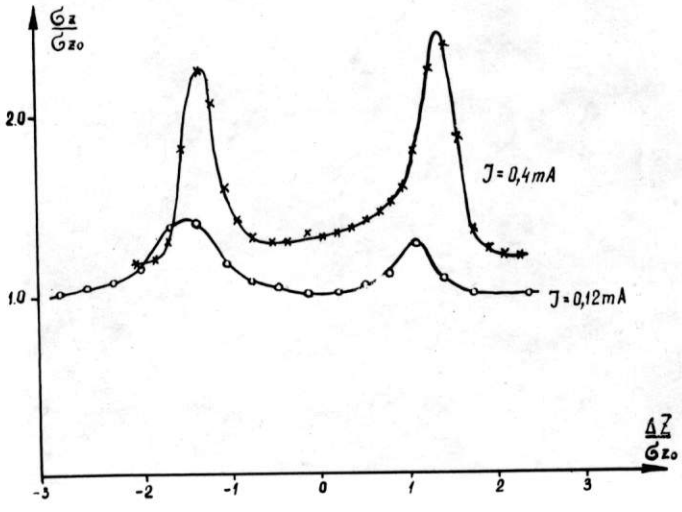

Fig. 3 A relative increase of the vertical size in respect to a relative separation of orbits at the interaction point.

The maximum luminosity at an energy of 1.85 GeV was 3×10^{28} cm^{-2} s^{-1} at the currents of 0.8×0.8 mA^2. The limiting linear tune-shift did not exceed 0.015. It is two times lower than the design value. Comparison of the luminosities at energies of 1.55 and 1.85 GeV gives approximately $L \sim \gamma^4$.

4. THE FIRST EXPERIMENTS

In March-April 1980 the first experiments on precision measurement of the masses of ψ and ψ' mesons were carried out at VEPP-4. For energy calibration the spin precession frequency was measured, because the ratio of precession frequency to revolution frequency is only dependent on particle energy and the anomalous magnetic moment of an electron. This method was previously used at the storage ring VEPP-2M (Ref. 3) for the calibration of the masses of ϕ and K mesons.

The energy calibration was done as follows. The electron beam was polarized in the booster ring of VEPP-3; the polarization time was about 1 hour. Then the polarized beam travelled to the ring of VEPP-4. The precession frequency was determined from the resonance depolarization of the polarized beam. The beam was resonantly affected by the transverse magnetic field with a smoothly varying frequency. The beam is depolarized if the precession frequency coincides with the variable field frequency. The beam depolarization was identified by a change in the counting rate of the particles escaping from the beam due to the internal scattering effect, while its cross-section depends on the degree of polarization.

The positions of the ψ and ψ' resonances were measured with the use of "OLYA". Seven cycles of measurements were carried out on the ψ resonance and five cycles on the ψ' resonance (Fig. 4). The storage ring energy was calibrated before each cycle and immediately after it.

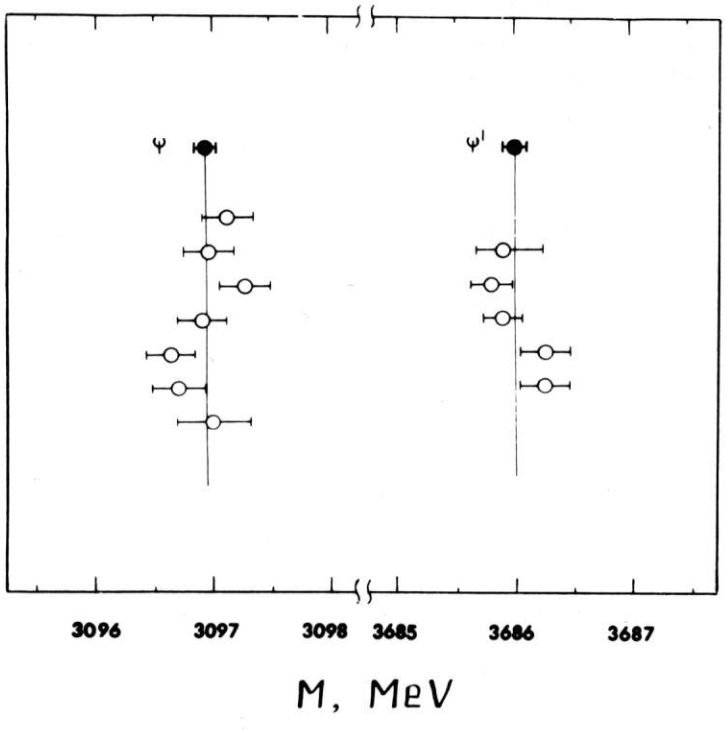

Fig. 4 The results of the measurement of masses and ψ and ψ' resonances.

After data processing and averaging over all cycles the masses of the resonances are as follows:

$$M_{\psi} = 3096.93 \pm 0.09 \text{ MeV}$$

$$M_{\psi'} = 3686.00 \pm 0.10 \text{ MeV} .$$

The above-described calibration procedure enables the accuracy of ψ and ψ' mass measurements to be improved by a factor of 20 in comparison with previous data.

5. PLANS

The detector MD-1 was scheduled for installation in the ring of VEPP-4 in late 1980. The beam energy will be increased to 2×5.5 GeV.

* * *

REFERENCES

1) I.Ya. Protopopov, Status report at the colliding electron-positron beam facility VEPP-4, Proc. 10th Int. Conf. on High-Energy Accelerators, Protvino (Serpukhov), 1977, Vol. 1, p. 421.

2) S.B. Vasserman et al., Starting of the positron-electron source for VEPP-4, Proc. 6th Nat. Conf. on Charged Particle Accelerators, Dubna, 1979, Vol. 1, p. 128.

3) G.M. Tumaikin, Proc. 10th Int. Conf. on High-Energy Accelerators, Protvino (Serpukhov), 1977, Vol. 1, p. 443.

4) S.D. Belov et al., Proc. 5th Nat. Conf. on Charged Particle Accelerators, Moscow, 1977, Vol. II, p. 291.

5) S.E. Baru et al., Magnetic detector MD-1, Preprint INP 77-75, Novosibirsk (1977).

6) G.I. Budker et al., Atomic Energy 44 (5), 397 (1978).

7) V.A. Sidorov, Proc. 1979 Int. Symp. on Lepton and Photon Interactions, Batavia, 1979 (FNAL, Batavia, 1980), p. 490.

THE ANTIPROTON TARGET STATION ON THE BASIS OF LITHIUM LENSES

B.F.Bayanov, A.D.Chernyakin, V.N.Karasyuc, G.I.Silvestrov,
T.A.Vsevolozhskaya, V.G.Volohov, G.S.Willewald

Institute of Nuclear Physics, Novosibirsk, USSR

ABSTRACT

In the paper we describe the project of an antiproton target station with particle focusing carried out with lithium lenses. The optimal conditions of obtaining high particle density inside a phase volume determined by the following antiproton cooling for three projects - Precooler (FNAL), Antiproton Accumulator (CERN) and INP-IHEP (USSR) are analysed. The efficiency of antiproton collection with a lithium lens is compared to the efficiency achieved with other focusing devices - magnetic horn and quadrupole triplet.

In all antiproton storage ring projects, the major problem of optimizing antiproton production conditions is the achievement of maximum phase density of particles in the phase volume determined by the requirements of a subsequent beam cooling. For this purpose, the geometrical parameters of a target, its material, and the conditions of proton beam focusing and antiproton collection should be optimized. The present paper concerns the optimal targetry conditions for three designs of antiproton storage rings - Precooler (FNAL), Antiproton Accumulator (CERN), and Antiproton Source for the IHEP Acceleration-Accumulator Facility (INP) and also the efficiency of antiproton collection by various optical devices.

The optimal targetry conditions analysis

The antiproton beam parameters at the target entrance are mainly determined by the antiproton production angles and a target length. The production angles distribution may be considered as a Gaussian one with the mean square $\langle\theta^2\rangle \cong \frac{2mm_\pi c^2}{p^2}$, ($m_\pi$ is the pion mass, m and p are the antiproton mass and momentum). This follows from the thermodynamical description of the antiproton transverse momentum distribution at $T \cong m_{\bar{p}}c^2$. This description agrees well enough with experimental data at relatively small angles. The antiproton distribution in a transverse phase space may be characterized by the effective values of an emittance $\varepsilon_{\bar{p}}$ and α and β - functions, which are determined by the mean squares of angles and coordinates, $\langle\theta^2\rangle$ and $\langle r^2\rangle$, and by the product $\langle r\theta\rangle$ at the target entrance as $\varepsilon_{\bar{p}} = \sqrt{\langle r^2\rangle\langle\theta^2\rangle - \langle r\theta\rangle^2}$, $\beta_{\bar{p}} = \frac{\langle r^2\rangle}{\varepsilon_{\bar{p}}}$, $\alpha = -\frac{\langle r\theta\rangle}{\varepsilon_{\bar{p}}}$. The values $\langle r^2\rangle$ and $\langle r\theta\rangle$ are $\langle r^2\rangle \cong \frac{\langle\theta^2\rangle z^2}{3}$ and $\langle r\theta\rangle \cong \frac{\langle\theta^2\rangle z}{2}$, where z is the target length.

The effective emittance of the antiproton beam and the minimum value of its β - function (at the centre of the target) are: $\varepsilon_{\bar{p}} \cong \frac{\langle\theta^2\rangle z}{2\sqrt{3}}$ and $\beta_{\bar{p},min} = \frac{z}{2\sqrt{3}}$. The antiproton yield is maximum when the target length is close to the nuclear absorption length λ . At $z = \lambda$, the emittance may

be considered as an effective emittance of antiproton production, $\varepsilon_0 = \frac{\langle\theta^2\rangle\lambda}{2\sqrt{3}}$. The capture efficiency at a given acceptance ε may be characterized by the function F determined by the relation of the acceptance to the antiproton beam emittance, the degree of proton and antiproton absorption inside the target. The number of captured antiprotons per incident proton is determined by means of this function as $\frac{\Delta N_{\bar{p}}}{N_p} = \frac{1}{\sigma_{in}} \cdot \frac{d\sigma}{dp} \cdot F \cdot \Delta p = \frac{1}{\sigma_{in}} \cdot \frac{d^2\sigma}{dp d\Omega} \pi \langle\theta^2\rangle F \cdot \Delta p$.

Analytical evaluation of the capture efficiency into the acceptance under condition that $\varepsilon \ll \lambda\langle\theta^2\rangle$ and the acceptance envelope function β equals to that of an antiproton beam $\beta_{\bar{p}}$, determines the optimal target length z_{opt} as $z_{opt} \cong 1.3\sqrt{\frac{\varepsilon\lambda}{\langle\theta^2\rangle} + \frac{r_0^2\lambda}{\varepsilon}}$ and corresponding value of F as:

$$F \cong \frac{8}{3} \cdot \frac{\varepsilon \cdot \exp(-\frac{z_{opt}}{\lambda})}{\langle\theta^2\rangle(\lambda + z_{opt})}$$

Here r_0 is the radius of a proton beam with the uniform particle density. The thin proton beam condition is $r_0^2 \ll \frac{8}{3} \cdot \frac{\varepsilon^2}{\langle\theta^2\rangle}$. The optimal antiproton collection angle is determined by a minimum value of β - function of the acceptance $\beta_{min} = \beta_{\bar{p},min} = \frac{z_{opt}}{2\sqrt{3}}$, and it equals to $\alpha_{max} \cong 1.65\left(\frac{\varepsilon\langle\theta^2\rangle}{\lambda}\right)^{1/4}$. The expression for $\frac{\Delta N_{\bar{p}}}{N_p}$ is $\frac{\Delta N_{\bar{p}}}{N_p} \cong \frac{1}{\sigma_{in}} \cdot \frac{8}{3}\pi\varepsilon\Delta p \cdot \frac{d^2\sigma}{dp d\Omega} \cdot \frac{\exp(-\frac{z_{opt}}{\lambda})}{z_{opt}+\lambda}$. In analytical evaluation of the capture efficiency we have not taken into account the multiple and elastic nuclear scattering of protons and antiprotons, the difference in their absorption lengths, the angular spread and the inhomogeneities of the proton coordinate distribution in the initial beam. It has been done in computer simulation; its results (Fig. 1, a-d) are consistent with the analytical estimates. The values of F in Fig. 1A, b were calculated at optimal β_ε and z (tungsten) for each value of ε and r_0, in Fig. 1c - for optimal z. Shown in Fig. 1d is the F dependence on a target length (mercury) for targets with a large cross-section and with a cross-section equal to that of a proton beam (thin target). The proton beam β - function values for the data in Fig. 1c, d are: 1 cm (FNAL), 6 cm (CERN), 10 cm (INP). The main parameters characterizing the optimal targetry for three above mentioned projects are listed in Table 1.

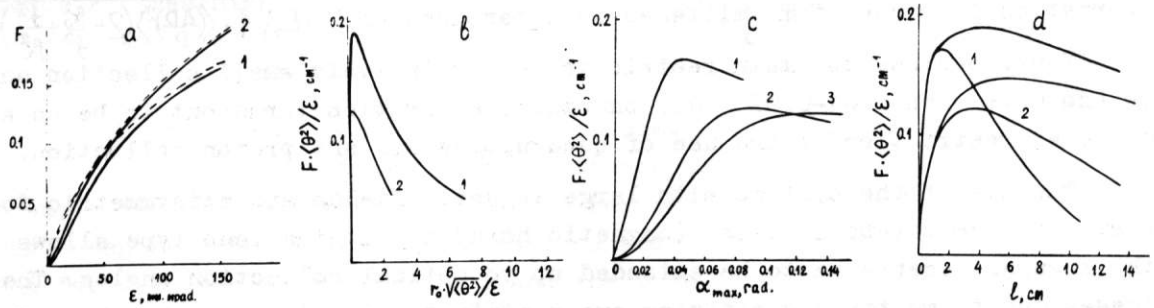

Fig. 1. Capture efficiency in the dependence on a) the acceptance size for the proton beam radius equal to 0.5 mm (1) and infinitely thin proton beam (2). Solid lines denote the simulation, dotted lines - analytical evaluation. The antiproton momentum is equal to 6 GeV; b) the proton beam radius for the FNAL (1) and AA (2) project; c) the collection angle from a target for the FNAL (1), INP (2), and AA (3) projects; d) the target length for the thick and thin targets at the uniform proton beam distribution, the FNAL (1), AA(2).

Table 1

	P GeV/c	ε mm.mrad	$\frac{\Delta p}{p}$,%	Target material	Z_{opt} cm	α_{max} mrad	F
FNAL[1]	4.5	5	±2	Hg W	1.5	35	0.0064 0.0086
CERN[2]	3.5	100	±0.75	Hg W	3.5	100	0.053 0.066
INP[3]	5.5	60	±3.2	W	3.5	80	0.080

Antiproton collection

Antiproton collection up to the optimal angle requires powerful optic systems. The choice of a collecting lens (quadrupoles, "magnetic horns", lithium lenses) is determined both by angular acceptance and aberrations, among which the chromatic aberration needs the great care.

The chromatic dispersion of particle deflection angles in a lens leads to an additional angular spread in the beam. If the beam transfer with an optical system is described with a matrix (M) as $(X)=(M)(X_0)$, the angular and coordinate increase at its entrance due to chromatic aberration (ΔX) is described by the matrix (M') obtained by differentiation of (M) over momentum, as $(\Delta X)=\frac{\Delta p}{p}(M')(X_0)$. The effective angular and coordinate increase in a beam source (ΔX_0) is determined as $(\Delta X_0)=(M)^{-1}(\Delta X)=\frac{\Delta p}{p}(M_0')(X_0)$, where $(M_0')=(M)^{-1}(M')$. An increase of beam emittance is described by the expression:

$$\varepsilon=\varepsilon_0\sqrt{1+\left\langle\left(\frac{\Delta p}{p}\right)^2\right\rangle\left(a_{11}^2+a_{22}^2+a_{21}^2\beta_0^2+\frac{a_{12}^2}{\beta_0^2}\right)+\left\langle\left(\frac{\Delta p}{p}\right)^2\right\rangle^2\cdot\Delta^2}$$

where a_{ik} and Δ are the elements and determinant of (M_0'). For example, the use of a quadrupole triplet, proposed to collect antiprotons with the momentum spread $\pm 1.5\cdot10^{-3}$ in a preliminary FNAL project[4], at the momentum spread $\pm 2\cdot10^{-2}$ would lead to a decrease of the capture efficiency by a factor of 4, as shown by computer simulation. For a thin lens with focal distance f the aberration increase of an emittance is determined as $\varepsilon=\varepsilon_0\sqrt{1+\left\langle\left(\frac{\Delta p}{p}\right)^2\right\rangle\left(2+\frac{\beta_0^2}{f^2}+\frac{f^2}{\beta_0^2}\right)}$.

Thus, besides the main restriction - a relatively small collection angle (no more than 0.01-0.02 rad), chromatic aberration turns out to be an additional restriction on the use of quadrupoles for antiproton collection.

The use of the systems with large magnetic fields and axisymmetric focusing of the parabolic lens (magnetic horn) or lithium lens type allows the angular acceptance to be extended up to optimal collection angles. The losses due to multiple scattering are minimized, in this case, by short focal lengths and minimum material thickness. Unfortunately, the nuclear interaction can limit the applicability of such systems in some cases.

Fig. 2 shows the profiles of possible variants of parabolic lenses for antiproton collection in the optimal angle in all three projects. These lenses have the focal distances, fields, and the wall thicknesses close to the limits. The currents in the lenses are: 150 kA (FNAL), 300 kA (CERN),

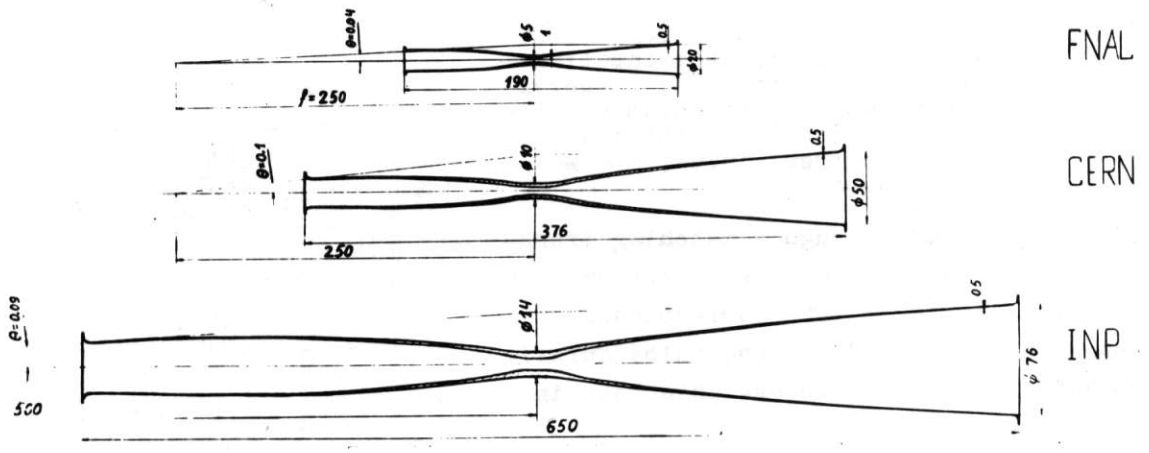

Fig. 2 Variants of parabolic lenses. Cross-section

400 kA (INP). The profile shapes are determined by the linear dependence of entrance coordinates on exit angles, that provides the minimum geometrical aberration[5]. The wall thickness changes with a distance from the axis as $\frac{1}{r}$ and is equal to 0.5 mm at maximum r. It corresponds to the mechanical stress $\sigma > 1200$ kg/cm^2 in the wall. The computer simulation of particles passage through aluminium lenses shows that the capture efficiency decreases by more than 4 times for the FNAL project ($F = 0.0015$) and by 1.65 times for the CERN project ($F = 0.032$). In the FNAL case the losses are mainly due to multiple scattering. The nuclear losses and chromatic aberration cause a decrease in efficiency of about 20%. In the CERN case, the decrease is largely (down to $F = 0.036$) due to nuclear losses.

An essential decrease of multiple scattering can be achieved with the use of lenses made of beryllium. The manufacturing process for beryllium lenses with the parameters close to those for FNAL and CERN projects has been developed in the INP[6]. In the FNAL case, the beryllium lens efficiency is about 2 times higher as compared to the aluminium one, i.e. the capture efficiency constitutes 0.5 from the maximum; in the CERN case, the gain is 6% only (up to $F = 0.034$).

Lithium lenses[7] can provide the minimum focal distance at which the distortion of the antiproton beam emittance is excluded nearly completely. For example, in the FNAL project the lens for antiproton collection at an optimal angle can have the 10 cm focal distance and the 0.8 cm aperture. In this case, the field on the surface is 12 T and the lens length is 6 cm. The angle of multiple scattering in the lithium and beryllium walls at the ends is $\sqrt{\langle\theta^2\rangle} = 7 \cdot 10^{-4}$ rad, that is less than the angular size of acceptance at the lens. Computer simulation shows that the losses in capture efficiency scarcely exceed nuclear losses in the lens. At INP the technology of lithium lenses has been developed, and wide experience has been gained in operation with similar systems[8]. At present, INP is designing the lens shown schematically in Fig. 3. It has aperture 2 cm, length 10 cm, and can be fed by a 800 μs current pulse

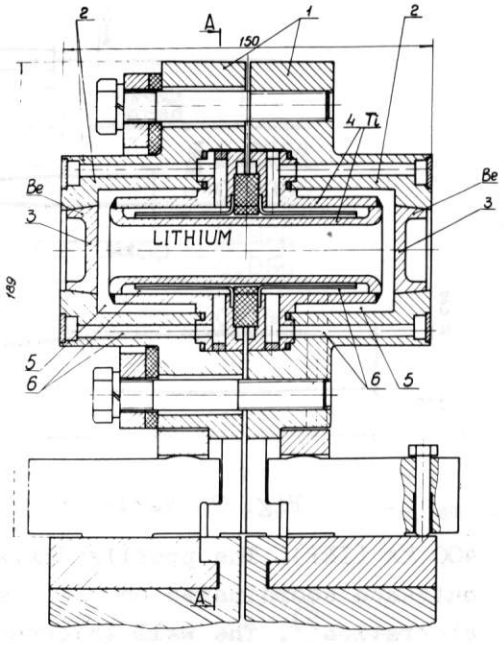

Fig. 3 The antiproton lithium lens cross-section: 1-flat current input; 2 - current connection cups; 3 -beryllium windows; 4 - titanium envelope of the lens, 5 - lithium axisymmetric current input; 6 - water cooling system.

of up to 700 kA through a matching transformer. Change in innermost structure (position 4 in Fig. 3) and corresponding change in the amplitude and pulse duration make it possible to use this lens in all three projects.

The focal distance of the collecting lens has a lower limit due to a burning through the beryllium entrance wall of the lens by a proton beam with high density near the target. Heating estimates and the FNAL neutrino beam experience with beryllium targets show that at an intensity of $3 \cdot 10^{13}$ protons per pulse and a millimeter beam size beryllium is not destroyed. To have such a size at a distance of about 7 cm from the target center, the proton beam should have large divergence achieved by strong focusing of it on the target. The lithium lens with the 35 cm focal distance and the 0.5 cm aperture meets this condition. For 80 GeV it has length 13 cm and field 15 T. At present, such a lens is undergoing a test at INP.

Proton focusing on a target and antiproton collection with lithium lenses with the above parameters results, for the FNAL project, in a capture efficiency constituting the $\sim$ 0.75 of the ideal value (Table I). If, because of the collecting lens entrance wall heating, it is necessary to shift it up to the focal distance of 20 cm, the scattering contribution decreases the collection efficiency down to $F = 0.0035$. This is only 10% higher than for the beryllium horn.

The target device

At intense proton beams (more than 10^{13} particles per pulse) and small beam spot sizes the work with heavy targets is accompanied by a large energy release (of the order of a few kJ) and high temperature of pulse heating; the latter leads to the explosive regime of a target operation. One of the ways to overcome the difficulties is the use of liquid-metallic, for example mercury, targets. This enables one to replace a target between pulses and to solve the problem of target cooling. After consideration of several variants of mercury targets we have chosen a flat-jet-like target. The jet flows through a narrow slit and the level of mercury is maintained constant with a pump. If the mercury level above the slit is 1-2 cm, the jet turns out to be

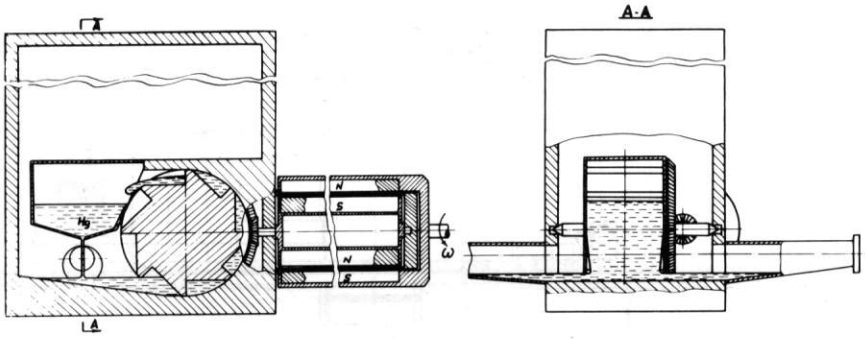

Fig. 4 Schematic cross-section of mercury pumps.

well-shaped with the stable cross-section. In studying the mercury jet flow from a narrow slit of 60 cm long its width ranged from 0.5 to 3 mm. After analysing various designs of pumps for mercury pumping we have chosen simplest variant the principle of operation of which is demonstrated in Fig. 4. The trials of the models of these pumps showed that, it can provide pump capacity more 5 liters per minute, sufficient for creating a stable jet with 60 x 3 mm^2 cross-section. This construction is placed in the air-tight containers with water cooling. The beam is passed through the exit and entrance windows covered with beryllium foils.

ATS layout

The use of short focusing lenses with small apertures allows a very compact antiproton target station (ATS) to be built up. The station scheme is shown in Fig. 5. All components of the station are placed on one common platform (4), 2 m long, and 0.7 m wide: a lithium lens for proton focusing (5), a target device (3), a lens for antiproton collection (2), and a bending magnet with the 5 T field. The platform can move along a stationary plate (10) together with the mobile section of shielding (7). As a plug, the latter enter the window of a stationary shielding (8,16) under operation of the ATS. Both lenses and separating magnet, with their matching transformers are installed on the platform and have radiation hard insulation. The transformers have a low-inductance current inputs (17) which pass through the mobile shielding. The current inputs are connected to a remotely-operated switch (15). Each element can be lifted up and shifted with a special manipulator for replacement. To do this, each element is mounted on the special catches and remotely-operated current and water connections. Both lenses can be remotely-adjusted simultaneously with an accuracy better than 100 microns.

The ATS will be mounted at IHEP for a study of the behaviour of solid and liquid metallic targets in the explosive regime at the 70 GeV proton beam and also for solution of a number of problems concerning the performance of a complex physical equipment at very high levels of radiation.

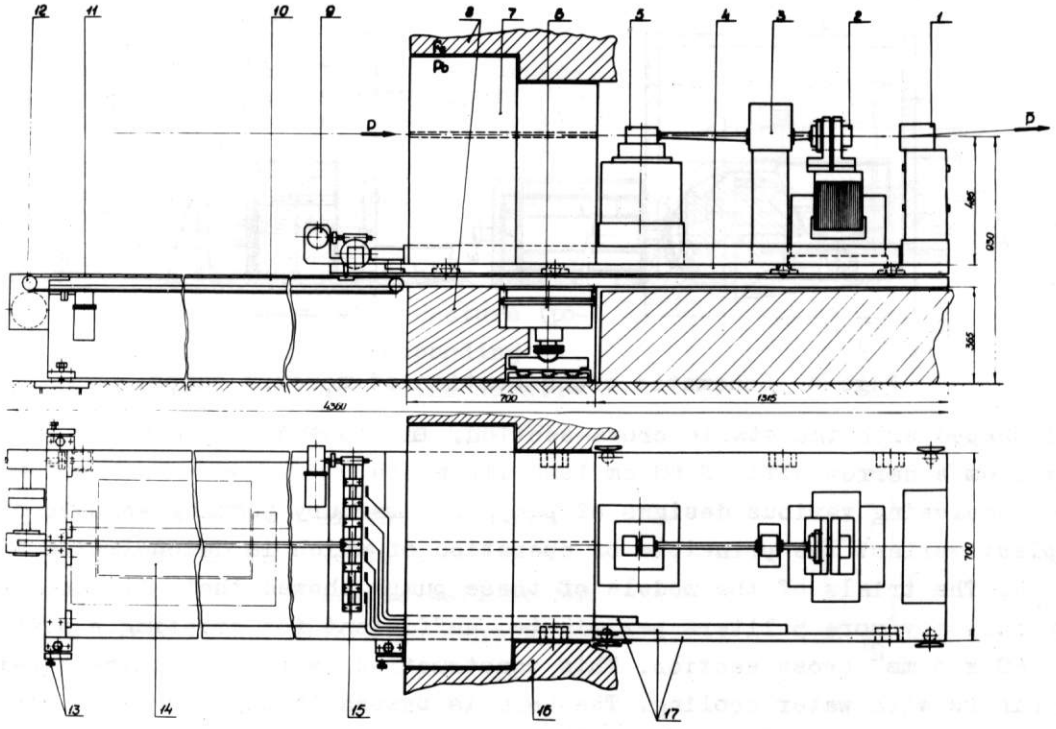

Fig. 5 ATS layout. 1 - bending magnet, 2 - antiproton lens, 3 - target device, 4 - mobile platform, 5 - proton lens, 6 - distant adjusting device of the ATS, 7 - mobile shielding, 8 and 16 - stationary shielding, 9 - switch-drive, 10 - stationary plate, 11 - chain belt, 12 - drive mechanism, 13 - adjusting devices, 14 - the second matching transformers, 15 - current switches, 17 - radiation hard current inputs.

* * *

REFERENCES

1. Design report. The Fermilab high-intensity antiproton source, FNAL, October, 1979.
2. Design study of a proton-antiproton colliding beam facility, CERN/PS/AA, 78-3, 27.1.1978.
3. T.A.Vsevolozhskaya et al., "An antiproton source for the IHEP acceleration-accumulation facility. INP Report, May 1980.
4. Beam Transport and Target System for pp and $p\bar{p}$ Colliding Beams, FNAL 06/20/78.
5. T.A.Vsevolozhskaya, G.I.Silvestrov, ZhETF, XLIII, 61, 1973.
6. G.S.Willewald, V.N.Karasyuk, G.I.Silvestrov, ZhETF, XLVIII, 566, 1978.
7. T.A.Vsevolozhskaya, M.A.Lyubimova, G.I.Silvestrov, ZhETF, XLV, 2494, 1975.
8. B.F.Bayanov, G.I.Silvestrov, ZhETF, XLVIII, 160, 1978.

STUDIES OF THE ELECTRON BEAM FOR THE FERMILAB ELECTRON COOLING EXPERIMENT

W. Kells, P. McIntyre, L. Oleksiuk*
Fermi National Accelerator Laboratory, Batavia, Illinois, USA.

N. Dikansky, I. Meshkov, V. Parkhomchuk
Institute for Nuclear Physics, Novosibirsk, USSR.

W. Herrmannsfeldt
Stanford Linear Accelerator Center, Stanford, California, USA.

ABSTRACT

The electron beam for the Fermilab Electron Cooling Experiment provides a cold (T_e ~ 1 eV) D.C. electron beam with 110 kV, 26A. Stable operation has been achieved up to 70 kV, 6A. A new mechanism for efficient beam collection and energy recovery is described. The beam is decelerated nearly to rest before entering the collector geometry. Providing the electric and magnetic fields obey several conditions in this region, residual gas ions trap stably on the space charge equipotentials, permit deceleration nearly to rest in vacuo, and suppress backscatter electrons from the collector surface. In this way we can reduce current losses to $\frac{\delta I}{I}$ ~ 2 x 10^{-4}, while recovering ~ 95% of the beam power.

1. INTRODUCTION

The $\bar{p}$ source at Fermilab will use electron cooling for the accumulation of precooled bunches of 200 MeV antiprotons[1]. The required electron cooling performance can be achieved using a cold electron beam with 110 kV, 5-10A. The electron cooling occurs in a long straight section of the Fermilab Electron Cooling Experiment, shown in Figure 1.

The electron beam design is described below. The beam has been operated stably up to 70 kV, 6A. Results of beam studies are presented, including beam position measurement, temperature measurement, and collection studies.

1.1 Electron Gun

The electron beam must have a rest frame temperature T_e < 1 eV. To produce such a low temperature, the electron gun has been designed with a classic Pierce geometry, and is itself immersed in the magnetic field. This means that the magnetic field lines thread through the cathode, and follow the electron trajectories all the way to the collector. Otherwise, the electrons would gyrate around the actual magnetic field direction, and increase greatly the transverse temperature. We have chosen to use the electron gun design developed for the SPEAR klystron. It produces a 28A, 27 cm^2 beam at 110 kV. The dispenser cathode can be reactivated repeatedly after exposure to air. The defocusing lens action of the anode causes the electrons to spiral, resulting in the undulation. This undulation is cancelled by a "resonant" focusing system of three electrodes. Electrode potentials are adjusted to match the spiral motion so that the electrons emerge parallel into the drift region.

1.2 Drift Region

After leaving the gun, the beam is bent 90° to superimpose it on the proton beam. The bending is accomplished with a crossed toroidal and dipole magnetic field. The resulting trajectory bends through a circular arc without exciting gyrations. The toroid has a gradient of 6.7 kG/m, and a dipole field of 80G.

The cooling will take place in a 5 m long drift region, where the electron beam is confined by a uniform-field solenoid. We have chosen a solenoidal field B_o = 1 kG as being adequate both for beam confinement and for studying "fast" cooling. The solenoid is an assembly of 0.5 m long coils of anodized aluminum strip conductor. The field produced by a long sequence of the coils with minimum spacing has a uniformity $(\delta B/B)_{rms} \leq 5 \times 10^{-4}$, sufficient for optimal electron cooling.

The ground potential surface throughout the bending and cooling region is a drift tube of 6" diameter. This drift tube is split longitudinally into segments, and each segment is connected to an independent voltage source (see Figure 1). By depressing the reference potential in the cooling region several kV below the ground in the short drift sections in each 60° bend, it is possible to trap the ions formed by beam gas scattering in the cooling regions, and neutralize the space charge in the electron beam.

1.3 Depressed Collector

After a second 90° bend, the beam is decelerated and absorbed in a collector assembly. It is essential to recover as much as possible of the beam power (2.6 MW) for realistic collection and optimum beam regulation. For this purpose the collector is operated at a potential only slightly

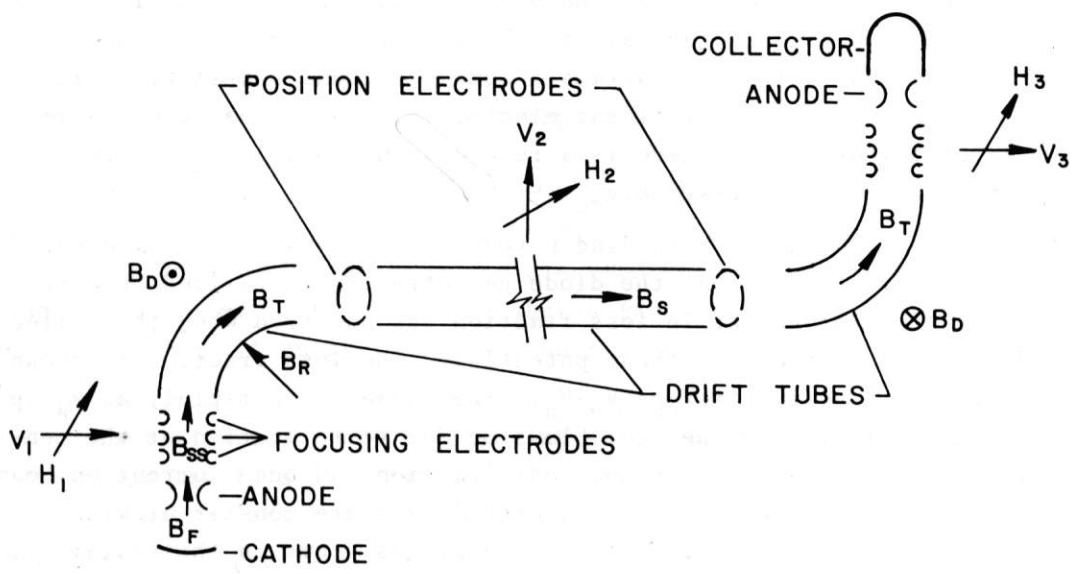

Figure 1. Schematic illustration of the electron beam system.

(δE ~ few kV) above that of the electron gun cathode. The collection is then efficient only if no electrons have lost more than δE of energy since their birth at the gun cathode. Any energy coupled to gyration in the deceleration process is difficult to recover into longitudinal motion. One difficulty in maximizing the collection efficiency at the collector is secondary emission and backscattering from the collector surface.

2. BEAM COLLECTION STUDIES

The early beam studies have been reported in detail elsewhere[2]. We will describe here the studies of the beam collection process, in which some interesting new features were observed.

The beam is decelerated nearly to rest in the collector, in order to recirculate the beam current to the cathode. Thus the power supply which maintains beam energy (cathode voltage) supplies only that current which is lost to the walls, and can be easily regulated to the degree ($\delta V/V \leq 10^{-4}$) necessary for electron cooling. The main beam current is returned from collector to cathode by an isolated booster supply (few kV, many amps).

Beam losses are monitored in several ways. The gun anode and collector anode represent the limiting apertures in the boundary geometry. Each anode is water cooled, and the current into (or out of) each anode is monitored. In addition, the currents to each drift tube section are monitored, and the total current I_L supplied from ground to the cathode measures the total beam loss.

In the design of the electron beam, the collector anode was to be maintained at or near ground potential, while the collector V_c was to be maintained near cathode potential V_e. The deceleration would thus occur in the diode geometry between anode and collector. In operation this mode of collection resulted in loss of ~3% of the beam to the anodes. This is interpreted as being the high energy tail of the spectrum of electrons backscattering from the (Cu) collector surface. Some electrons backscatter with nearly the full energy of an incident electron[3], and can be accelerated out of the collector unless there is a retarding potential of the same order as the collector depression. $V_{cc} = V_e - V_c$.

The only way to make a retarding potential is to vary the collector anode voltage V_a. In this way the diode geometry is generalized to a triode. A dramatic improvement in loss fraction was observed when the collector anode was operated near cathode potential. The loss fraction is shown in Figure 2 as a function of $V_{ca} = V_e - V_a$. The losses drop rapidly as V_a approaches V_e, until finally the beam blows up due to reflection of the central ray. The dependence of minimum loss fraction and beam current on beam energy is shown in Figure 3. The remaining losses are consistent with a calculation of outscattering from the residual gas atoms in the system (dashed line).

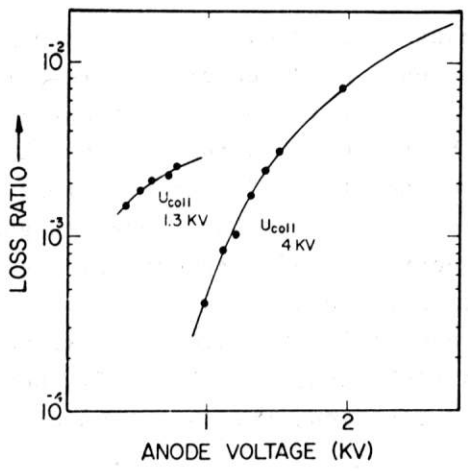

Figure 2. Loss fraction vs. V_a

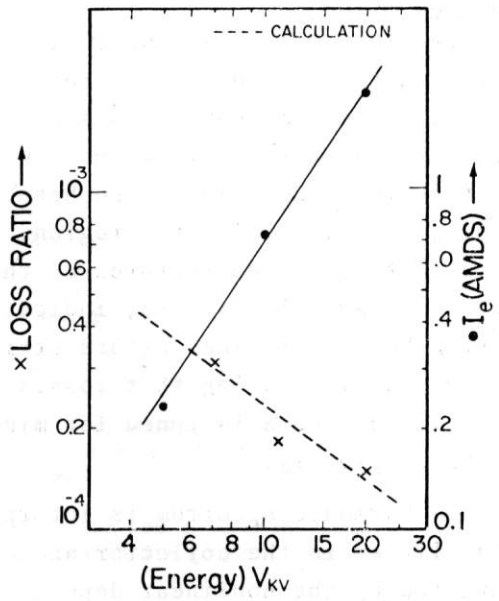

Figure 3. Loss fraction and I_e vs. V_e

This behavior was startling in view of our Poisson calculations of the beam trajectories in the collector region. The electron space charge for a 2A beam should produce a ~5kV depression in the aperture of the collector, and reflect central rays if $V_{ca} \lesssim 5$kV. The observed improvement for small V_{ca} signals the presence of a stable cloud of slow gas ions, which are formed and trapped in the potential well near the collector anode. The ion cloud naturally neutralizes the electron beam as it decelerates.

Ion trapping in the collector region has not been reported in electron beams at Novosibirsk and CERN. The dramatic effect on losses must result from a strong, uniform barrier to suppress backscattered electrons. This conclusion is substantiated in Poisson calculations that include ion neutralization.[1,2] For a fixed ion density, Poisson solutions show that a threshold current ~2A is required to create trapping wells. Electric and magnetic fields must be slowly varying (small radial components) in the collector anode region, to avoid leakage channels from the ion clouds to the anode. Diffusion to the walls must also be minimized. It is necessary for this reason to reduce ion heating by the electron beam, by allowing the magnetic guide field to terminate in an adiabatic fashion. The electron drag force and diffusion are then averaged away on successive spirals of gyromotion.[2]

The optimum loss fraction does not depend strongly on collector depression V_{cc} (see Figure2). We interpret this to mean that, while the topology of the equipotentials is altered by ion trapping, the total retarding potential near the collector scales with V_{cc}. Thus backscatters are suppressed independent of V_{cc}.

Beam tuning and collection have been studied over the range $20 < V_e < 70$ kV $2 < I_e < 7$ A. The loss fraction is $\sim 1\text{-}3 \times 10^{-4}$ for the entire range of energies and currents studied.

3. BEAM LOSS MECHANISMS

Beam loss mechanisms were studied by means of an RF antenna structure located in the long drift section. Two components of RF power spectra were observed. One component consisted of integral harmonics of a fundamental frequency $f_o = \sqrt{V_e/2L^2}$ (few MHz), which is the frequency with which an electron travels round-trip in the beam. This component was due to electrons escaping from the collector region, and bouncing back and forth between gun and collector. Three features of this component were of interest: 1) the Q of the low harmonics was ~8, indicating that on the average a reflected electron bounces 8 times before striking an anode; 2) The harmonics extend up to h~100, indicating that losses occur in tight charge packets; 3) when the collector anode is tuned for minimum loss fraction, this spectrum disappears completely.

The harmonic spectrum is interpreted as arising from electron-ion instabilities in the collector anode region. This interpretation is substantiated by the nonlinear dependence of RF power on loss current, shown in Figure 4.

The second component consists of a Doppler-spread spectrum centered on the gyrofrequency $\omega_o = eB/mc$ (~2 GHz). This component is the signal induced on the drift tube walls by each electron as it spirals around a field line. The power in the induced signal is proportional to the transverse temperature of the beam, and is used as a diagnostic during tuning studies.

* * *

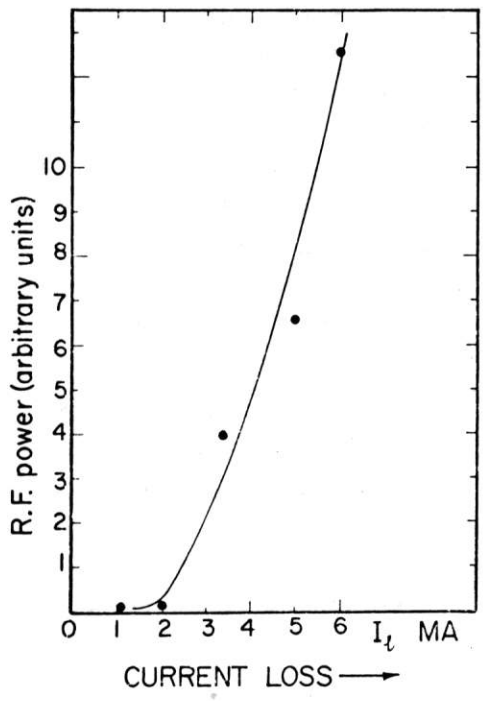

Figure 4. RF power vs. loss fraction.

REFERENCES

1) Design Report, Tevatron I. Fermilab (1980).

2) W. Kells et al., The Electron Beam for the Fermilab Electron Cooling Experiment, Fermilab TM-918(1980)

3) E.J. Sternglass, Phys.Rev.95,345 (1974).